

# Estimation of Brake Friction Coefficient for Blending Function of Base Braking Control

## Abstract

The brake architecture of hybrid and full electric vehicle includes the distinctive function of brake blending. Known approaches draw upon the maximum energy recuperation strategy and neglect the operation mode of friction brakes. Within this framework, an efficient control of the blending functions is demanded to compensate external disturbances induced by unpredictable variations of the pad disc friction coefficient. In addition, the control demand distribution between the conventional frictional brake system and the electric motors can incur failures that compromise the frictional braking performance and safety. However, deviation of friction coefficient value given in controller from actual one can induce undesirable deterioration of brake control functions. The main objective of the presented study is to propose a method to compensate disturbances induced by variations of brake linings friction coefficient through modifications of the brake torque demand for the enhancement of both brake performance and active safety.

The achievement of a compensation mechanism requires the estimation of relevant vehicle states. Hereunto, a novel technique based on a linear Kalman observer is proposed for the online estimation of the brake friction coefficient by relying upon the wheel speed sensors and inertia measurement unit (IMU). Such a tool enables a more efficient use of the frictional brakes aimed at minimizing losses of friction coefficient by keeping them in the optimal operational conditions. A simulation analysis will be carried out using the commercial vehicle dynamics simulation software IPG CarMaker to test the functionality of the developed estimator in the real-time mode. Experimental results from brake dynamometric test rig will be considered in the vehicle dynamics simulation software to reproduce the real behaviour of brake linings friction coefficient. The resulting improvements in brake control functions will be analysed against longitudinal base braking cases involving blending functions also in presence of failure of the electric motors.

## Introduction

In the recent years, the decoupled electrohydraulic brake system (EHB) has had a wide application in automotive brake design [1] [2] [3]. The lack of a direct hydraulic connection between the brake pedal and brake callipers guarantees additional degrees of freedom in the brake pressure actuation and reveals necessary for the proper enabling and control of the brake blending function in electric vehicles [4]. Whilst the development of strategies for brake torque distribution in

electric vehicle is a widely known research topic [5] [6], the compensation of disturbances during base brake manoeuvres is still a poorly investigated function. The external disturbances induced by variations of brake linings coefficient of friction can lead to unpredictable vehicle behaviour, which in turns affects the brake blending control process. Therefore, it is expectable that the disturbance compensation through the variation of the brake pressure actuation leads to the enhancement of braking performance and vehicle safety.

Indeed, in braking system control algorithms, the knowledge of brake linings coefficient of friction plays a crucial role. Deviation of its value given in controller from actual one can induce undesirable deterioration of brake control functions. A large set of phenomena occurring between the brake pad and disc affects the brake effectiveness and the dynamics of the pad-disc contact causing a wide variation of the friction coefficient: brake fading [7], [8], brake bedding [9], brake hysteresis against the pressure [10], brake hysteresis against the speed [11], brake wear [12] and aging [9], dependence against the environmental conditions [13] etc. The knowledge of the actual brake friction coefficient results in an accurate control of the frictional braking torque and allows the enhancement of both base brake functions, brake blending and regenerative braking control. In addition, the knowledge of the brake friction coefficient reveals also useful to guarantee failsafe operation and maintain the brake in the safe operating region by avoiding the fading.

Unfortunately, the influence of the previously listed phenomena on frictional interaction between brake disc and pad cannot be evaluated in real-time mode due to the complexity of known model-based approaches. Therefore, the present work proposes an estimator of the brake linings coefficient of friction that draws upon a linear Kalman filter of the wheel torque. The Kalman filter is widely used as system state observer because it ensures good robustness for tolerating differences between models and real dynamics of the vehicle, variations of model parameters and signal errors [14]. In its intent, the state observer outperforms classical analytical methods and reveals suitable for online applications by guaranteeing robustness of the estimation against changing road conditions and reliability against changes of the plant characteristics due to brake wear and aging, or in case of replacement with aftermarket brake linings. Afterwards, a compensation control function is developed in order to mitigate the external disturbances that affect the brake blending performance and driving safety of electric vehicles during base braking control.

The developed observer and estimator are assessed against a reference vehicle model from the commercial software IPG

CarMaker. Owing to the absence of an embedded model for brake friction generation, experimental results from brake dynamometric test rig are considered in the vehicle dynamics simulation software to reproduce the real behaviour of the brake linings coefficient of friction. The simulations are performed for an electric vehicle equipped with an electrohydraulic brake system and individual in-wheel electric motors. The transition from the friction braking to the electric braking or vice-versa has a remarkable impact on the brake performance. Its analysis reveals necessary in case of disabled regenerative braking function (e.g. fully charged battery) or failure occurrence. It is expectable that the knowledge of the brake friction coefficient enables an optimal intervention control of the conventional brake and a better monitoring of its working conditions. The obtained results

represent functionality of the developed estimator in real-time mode.

The paper comprises the following parts. In the next section the controller and its functional blocks are presented. In the second section the selected method for state estimation is put forth and validated against the vehicle dynamics simulator for different driving manoeuvres. In the third section, the estimation method for the brake linings coefficient of friction is put forth and validated. At last, the procedures for compensation of disturbances induced by variations in the coefficient of friction are illustrated for different blending configurations.

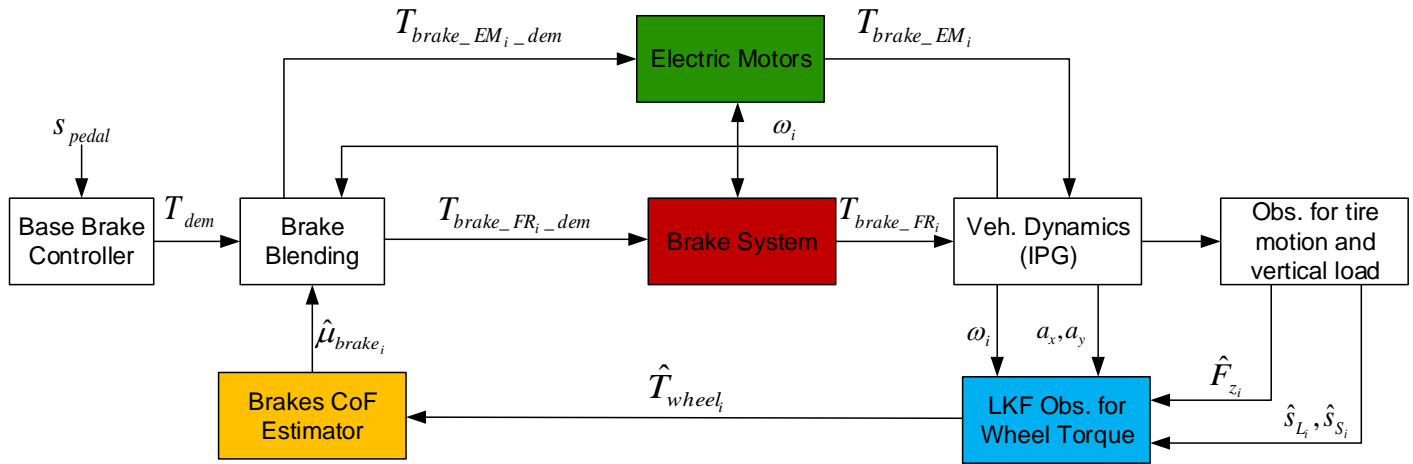


Figure 1. Overall scheme of the implemented controller with enabled blending function and friction compensation during base braking. The main blocks are reported in colours and associated detailed descriptions can be found in the text.

## Control structure

The employed controller is suited to a full electric vehicle equipped with individual in-wheel electric motors (IWM) and an electrohydraulic brake system (EHB) that cooperate to perform braking actions. The structure of the employed control is schematically reported in the Figure 1. From now on, the  $i$  index will be used to identify the four tyres:  $fl$ ,  $fr$ ,  $rl$ ,  $rr$ . The hat symbol " $\hat{\cdot}$ " will be instead used to represent an estimated or observed quantity. A reference vehicle deceleration map [15], as a function of the brake pedal travel  $s_{pedal}$ , is used in the Base Brake Controller in order to derive the demanded vehicle braking torque  $T_{dem}$ . The Brake Blending block is liable for the coordination between the friction brake system and electric motors by providing the demanded torque signals, respectively  $T_{brake\_FR\_i\_dem}$  and  $T_{brake\_EM\_i\_dem}$ , to achieve the demanded deceleration. Thanks to the feedforward configuration of the control system, once the load distribution is defined, it results trivial to evaluate the effective regenerative brake component

$T_{brake\_EM\_i}$  and the frictional brake torque  $T_{brake\_FR\_i}$  for each wheel. Afterwards, a linear Kalman filter is liable for the observation of the wheel torque  $\hat{T}_{wheel\_i}$  that in turns is necessary to estimate the brake linings coefficient of friction  $\hat{\mu}_{brake\_i}$ . The observer of the wheel torque relies on measurement coming from the vehicle sensors, viz. wheels speed  $\omega_i$ , longitudinal acceleration  $a_x$  and lateral acceleration  $a_y$ , and on-board estimates of the tyres vertical loads  $\hat{F}_{z_i}$ , longitudinal slips  $\hat{s}_{L_i}$  and side slips  $\hat{s}_{S_i}$ .

Brake friction losses owing to brakes warming up and fading occurrence can arise after a set of brake applications. The compensation of disturbances induced by friction coefficient variation is realized by updating the brake torque demand. The estimated brake linings friction coefficient is used in the calculation procedure for the conversion of the brake torque demand of frictional brakes to the pressure demand, which is then sent to the EHB system. The inputs of the controller are signals from the set of sensors measuring the wheel speeds,

electric motor current, brake pedal position, vehicle longitudinal and lateral acceleration and the brake pressure received from the EHB control unit. An accurate description of each functional block is provided in the following sections.

### Blending function of base brake control

The base-brake controller generates the torque demand to achieve the reference deceleration. The value of reference deceleration can be extracted from the brake pedal displacement sensor in accordance with the Figure 2, so that the torque demand can be calculated in accordance with eq. (1).

$$T_{dem} = m_v \cdot a_x^{ref}(s_{pedal}) \cdot r_w \quad (1)$$

Wherein,  $m_v$  represents the mass of the vehicle,  $a_x^{ref}$  is the reference deceleration as function of the brake pedal displacement  $s_{pedal}$ , and  $r_w$  represent the wheel radius. The brake blending factor  $\alpha$  is defined in order to allocate the demanded intervention level between the conventional brake system  $T_{brake\_FR\_dem}$  and the electric motors  $T_{brake\_EM\_dem}$ , in compliance with the Equation (2).

$$T_{dem} = \alpha \cdot T_{brake\_EM\_dem} + (1 - \alpha) \cdot T_{brake\_FR\_dem} \quad (2)$$

The defined torque demands are used to generate the control signals, whose actuation must undergo the physical system limits of both the frictional brakes and electric motors. It is worth noticing that limitations in the gradient of generation of wheel brake torque for both the electrohydraulic and electric brake system must be considered. The rate limit of pressure build-up towards the brake callipers is simulated with a second order transfer function as reported in [16]. Instead, the rate limit affecting the generation of the regenerative torque is rendered by means of a first order transfer function similarly to [4]. The knowledge of the estimated brake linings coefficient of friction allows calculating a brake pressure control signal. The torque exerted by the electric motors, generally equal to the demanded value, must comply a threshold value depending on the motor rotational speed and battery state of charge (SOC).

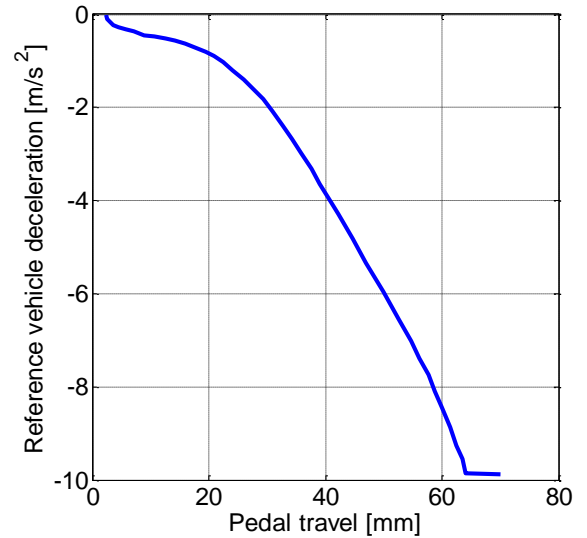


Figure 2. Reference vehicle deceleration map implemented in the Base Brake Controller

### Model simulation

In the present paper, the wheel torque observer and the friction coefficient estimator are assessed against a baseline vehicle simulated in IPG CarMaker. The Pacejka Magic formula tire model [17] is employed to depict the road-vehicle contact forces with effectiveness and low computational burden. The model includes also aerodynamic forces, nonlinear suspension model, steering system, decoupled electrohydraulic brake system. Owing to the absence of an embedded model for brake friction generation, the dynamic model [18] is used to reproduce the real behaviour of brake linings friction coefficient in the vehicle dynamics simulation software, previously calibrated against the experimental results obtained from brake dynamometric test rig at the Technische Universität Ilmenau.

### Vehicle model

The simulation results concern a full electric vehicle with all-wheel drive powertrain including individual electric in-wheel motors and decoupled electrohydraulic brake system. The vehicle parameters are reported in the Table 1.

Table 1. Vehicle configuration

Vehicle type	Passenger full electric vehicle
Total vehicle mass	1463 kg
Powertrain type	AWD
Drivetrain type	Individual in-wheel type motors without reduction gear
Brake System type	Decoupled electrohydraulic
Tyre size	195/65 R15

## Model of Electric Vehicle Powertrain

For the purpose of the study here presented, the electric powertrain includes individual in-wheel electric motors with possibility of enabling the regenerative braking mode with controllable power split between conventional and electric systems. The behaviour of the electric motors during the braking phases is modelled through a look-up table emulating the steady-state behaviour and a first-order transfer function for reproducing the transient behaviour.

## Model of the Brake System

The real behaviour of brake linings friction coefficient in the vehicle dynamics simulation software is modelled through the Ostermeyer model [18]. This latter is based on two differential equations in the friction and temperature states and captures the dynamical behaviour of the friction and its dependence against the temperature. This encompasses the fading and the hysteretic effect of the brake system. As reported in [18], the model relies upon the following set of differential equations

$$\dot{\mu} = -[b \cdot (Nv + \varepsilon)\mu - a \cdot T] \quad (3)$$

$$\dot{T} = -c[(T - T_0) - \gamma \cdot Nv] \quad (4)$$

For a more detailed description of the Ostermeyer model, please refer to [18]. Herein it is worth remarking that: (i) the group  $(Nv)$  represents the magnitude of the combination between the normal load and the speed; (ii)  $a, b, c, \gamma, \varepsilon$  are constant parameters linked to the pad chemical composition to be calibrated against experimental data; (iii)  $\mu$  represent the pad-disc friction coefficient; (iv)  $T$  stands for the disc contact temperature, where  $T_0$  is its initial state.

An assessment of the Ostermeyer's model presented here, consisting in its identification and validation against the experimental data acquired on the brake rig at the Technische Universität Ilmenau [19]. The acquired data correspond to the two tests reported in the Figure 3 for fixed constant sliding speed and oscillating input brake pressure.

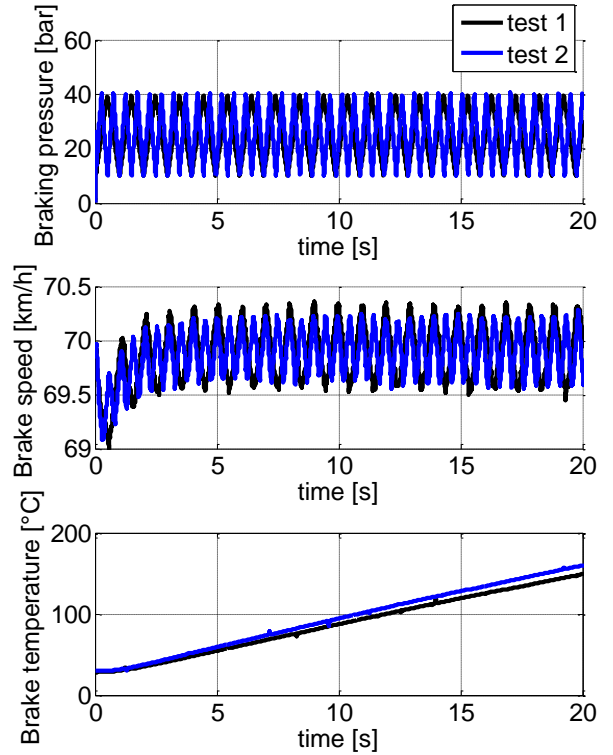


Figure 3. Experimental test conducted on the brake test rig at the Technische Universität Ilmenau whereby the test 2 features a double operating frequency compared to test 1.

During such a testing procedure, the brakes undergo increasing temperature, which significantly affects the brake performance. The dynamic model represented by the Equation (3) and (4) has been firstly identified against the first set of experimental data (Test 1) and then validated against the second data set (Test 2). The fitting was achieved by solving an optimization problem whose input variables are the model parameters  $a, b, c, \gamma, \varepsilon$ . To this regard, a minimization algorithm based on the Newton's method has been applied [20].

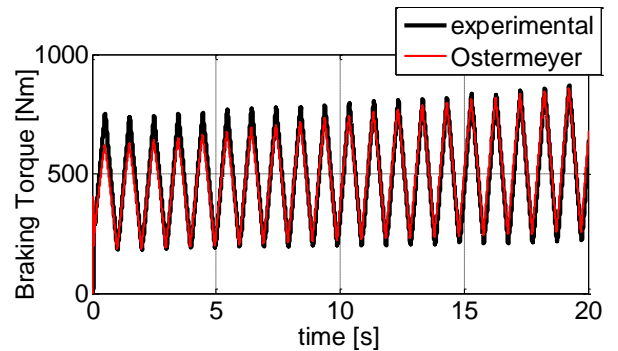


Figure 4. Identification result of the Ostermeyer's model against the Test 1 data set.

In Figure 4, the comparison between the experimental and the model predicted braking torque is reported. It is noticeable that, even in presence of increasing temperature value, the simulated profile does not depart from the reference. This confirms that the model under discussion takes into account the friction dependence against the temperature.

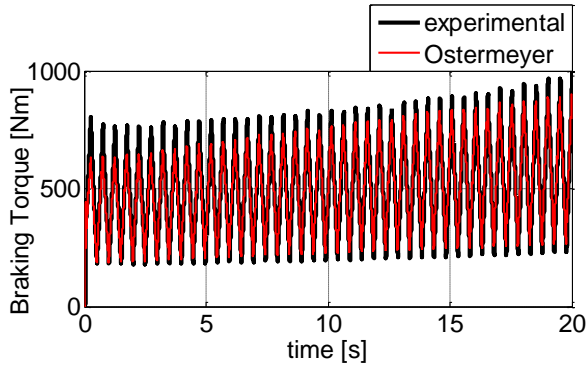


Figure 5. Validation result of the Ostermeyer's model against the Test 2 data set.

In the Figure 5 is instead reported the validation test performed against the second data set. Although a lack of accuracy is noticeable in correspondence of low temperature values (first half of the profile in diagram), the model exhibits a good overall prediction capability even in presence of increased pressure actuation frequency. Moreover, the model reveals capable to catch an increase of the average brake torque induced by the brake warming up.

## Wheel torque observer

The literature research effort of recent years has demonstrated that the state observation technique in all the engineering fields represents a valid substitute to the model based approach. The observation of the tire-road friction coefficient [21], [22], [23] and tire forces [24], [25] has been topic of great interest among the vehicle dynamics control community. What is common among these methods is that available vehicle sensors are used to estimate tire/road information based on the state variables of the wheels and the vehicle. In comparison to the above listed methodologies, the represented observer features an augmented state vector based on the wheels dynamics and a tyre model. Hence, the state space formulation associated with the observer is rearranged in order to handle the wheel torque as an augmented state [26] and guarantee the observability condition [27].

## Estimation Process

The observer state-space formulation stems from a quarter-car model for the vehicle longitudinal and lateral dynamics with fixed parameters. With reference to Figure 6, the proposed tool relies on the signals coming from the chassis accelerometer and the wheel speed sensors, reported as blue blocks, and on three units, represented as orange blocks. The KF combines information coming from models (prediction step) and sensors (update step), in presence of uncertainty, to provide a minimum variance estimation of the system state variables.

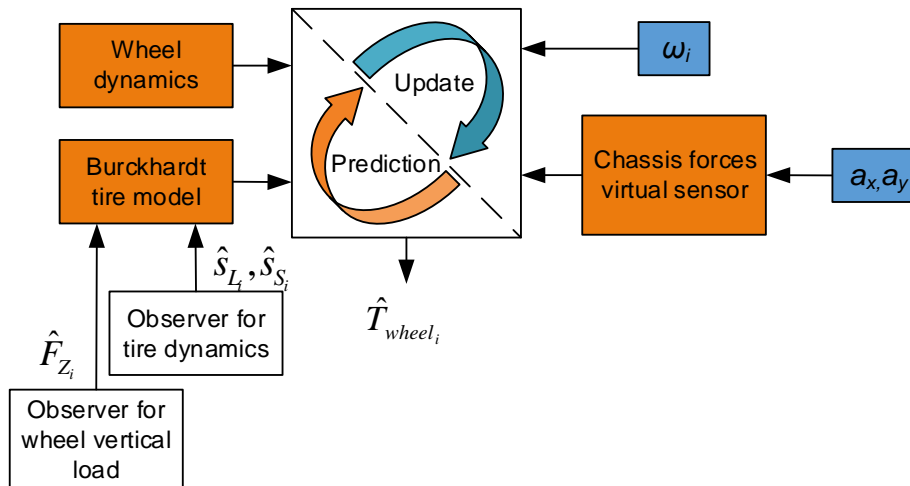


Figure 6. Scheme of the proposed linear wheel-torque observer: the update part is based on the measurements coming from the wheel speed sensors ( $\omega_i$ ) and chassis accelerometers ( $a_x, a_y$ ); the prediction part relies on the wheels dynamics equations and on the Burckhardt tire model [28] that, in turn, requires the knowledge of tire slip coefficients ( $\hat{s}_{Li}, \hat{s}_{Si}$ ) and the vertical load ( $\hat{F}_{Zi}$ ).

The filter state, measurement and input vectors are defined in the eq. (5)-(7) for the generic time step  $k$ . In addition, the

dynamics of the state variables is derived in compliance with the discrete state space set of equations (8a)-(8d) as follows:

$$x_k = \{\omega_{i,k}, \dot{\omega}_{i,k}, F_{Li,k}, T_{wheel_{i,k}}\}_{16 \times 1}^T \quad (5)$$

$$z_k = \{\omega_{i,k}^S, F_{Li,k}^{VS}\}_{8 \times 1}^T \quad (6)$$

$$u_k = \{\dot{F}_{Li,k}\}_{4 \times 1}^T \quad (7)$$

$$\begin{cases} \omega_{i,k+1} = \omega_{i,k} + \Delta t \cdot \dot{\omega}_{i,k} \\ \dot{\omega}_{i,k+1} = \frac{T_{wheel_{i,k}} - F_{Li,k} r_\omega}{I_\omega} \\ F_{Li,k+1} = F_{Li,k} + \Delta t \cdot \underbrace{\dot{F}_{Li,k}}_{input} \\ T_{wheel_{i,k+1}} = T_{wheel_{i,k}} \end{cases} \quad \begin{matrix} (8a) \\ (8b) \\ (8c) \\ (8d) \end{matrix}$$

The aforementioned system of equations constitutes the observer process model in discrete time formulation, wherein  $\Delta t$  is a small discrete time step. In compliance with the latter set of eq., the hub speed of each wheel  $\omega_{i,k}$ , is updated through (8a) once its derivative  $\dot{\omega}_i$  is known from the wheel dynamics of eq.(8b); wherein  $I_\omega$  is the wheel inertia and  $r_\omega$  is the wheel radius,  $T_{wheel_i}$  is the torque exerted on the wheel hub,  $F_{Li}$  represents the wheel longitudinal force. For the sake of convenience, the rolling resistance is included in the longitudinal tyre force in order to keep a time-invariant system. The longitudinal wheel force ( $F_{Li}$ ) is updated by providing its derivative as system input  $u_k$  to the eq. (8c). This latter relies on the Burckhardt tyre model with fixed parameters as a function of the wheel slips ( $\hat{s}_{Li}, \hat{s}_{Si}$ ) and the vertical forces ( $\hat{F}_{Zi}$ ). For a better understanding of the Burckhardt model, please refer to [28]. The vertical wheel loads and the slip ratios, in turn, are observed in accordance with the methodologies reported respectively in [29] and [28]. At last, in (8d), a random walk approach is used for the wheel torque state  $T_{wheel_{i,k}}$ ; it will be then corrected in the update phase.

With regard to the update part, the virtual sensor estimates the chassis longitudinal ( $F_x^{VS}$ ) and lateral ( $F_y^{VS}$ ) forces by drawing upon the measured longitudinal ( $a_x$ ) and lateral ( $a_y$ ) accelerations in accordance with the following eq. (9) and (10):

$$F_x^{VS} = m_v a_x - F_{R_x} \quad (9)$$

$$F_y^{VS} = m_v a_y \quad (10)$$

where,  $m_v$  is the mass of the vehicle and  $F_{R_x}$  is the sum of the forces opposed to the vehicle motion, namely the rolling resistance and the air drag force. The output vector  $z_k$  leading the observer update phase is constituted by the wheel speed sensors measurement  $\omega_i^S$ , and the virtually estimated longitudinal force for each wheel  $F_{Li}^{VS}$ .

At this point, two issues arise, which humper a correct observation of the system state. In the first instance, eq. (9) and eq. (10) provide a single value of longitudinal and lateral forces, which act on the entire vehicle. Hence, a correction factor  $K$  is defined, resulting from the combination of the tire model  $F_g^{TM}$  and virtual sensor  $F_g^{VS}$  (Figure 7). As specified in

the next section, this assumption provides the observer with compensation capability against changing road conditions. In the second instance, the virtually estimated and model-predicted components of the tyre force lean on two different reference systems, respectively the chassis-accelerometer and the tyre-model (Figure 8). The virtually estimated and predicted longitudinal components of the tyre force must be rotated onto the same reference. For simplicity reasons, the wheel reference is selected as the target; as shown in the Figure 8, the sideslip angle  $\alpha_i$  and the steering angle  $\delta$  must be taken into account. Hence, the translation matrix  $\bar{A}(\alpha_i, \delta)$  is defined and the following relation is stated:

$$\begin{Bmatrix} F_{Li}^{VS} \\ F_{Si}^{VS} \end{Bmatrix} = \bar{A}(\alpha_i, \delta) \begin{Bmatrix} F_{xi}^{VS} \\ F_{yi}^{VS} \end{Bmatrix} \quad (11)$$

A thorough analytical formulation of the previous eq. can be found in [28].

### Compensation against varying road friction coefficient

In order to solve the first problem, a correction factor  $K$  is introduced to apportion the virtually estimated longitudinal and lateral forces on each wheel. Looking at Figure 7, the correction factor stems from the definition of two global chassis forces, namely the global virtually estimated  $F_g^{VS}$  and modelled  $F_g^{TM}$  body forces. The following equations, (12) - (14), are applied:

$$K = \frac{F_g^{VS}}{F_g^{TM}} = \frac{\sqrt{(F_x^{VS})^2 + (F_y^{VS})^2}}{\sqrt{(F_x^{TM})^2 + (F_y^{TM})^2}} \quad (12)$$

$$F_{xi}^{VS} = K \cdot F_{xi}^{TM} \quad (13)$$

$$F_{yi}^{VS} = K \cdot F_{yi}^{TM} \quad (14)$$

The factor  $K$  is liable for compensating disturbances induced by unexpected variation of road conditions. The estimation of the correction factor is the key element of the adaptability of the linear observer against varying road conditions. Indeed, the virtually estimated forces are used to close the observer loop and update the final longitudinal force estimation. The modelled body forces come from the tyre model with fixed parameters; therefore, in case of changing road conditions it is expectable that the model prediction differs from the virtually estimated forces. The correction factor takes into account the difference between the modelled and virtually measured forces and is used for the correction procedure within the linear Kalman filter. A filter based on RLS (recursive least square) method is applied across a finite set of time steps in order to mitigate rapid variations of the correction factor  $K$ . As a consequence, the observer adaptation time against changing road conditions depends on the setting parameters of the RLS filter.

It is worth underlining that due to the chosen tyre model, the tyres slip factors lead the direction of the wheel forces. In addition, the direct proportionality imposed by the previous

equations, (13) and (14), explains why both the modelled and virtually estimated global body forces point in the same direction as reported in Figure 7.

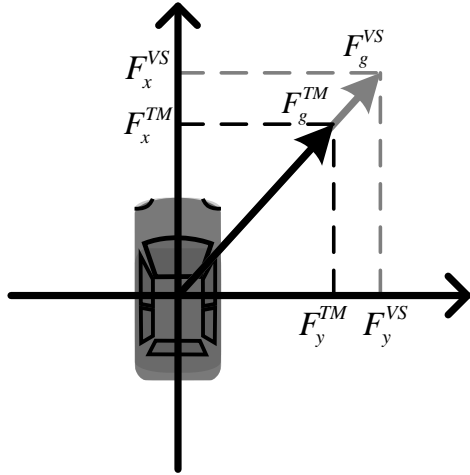


Figure 7. Representation of the global body forces and associated components with reference to the model (TM) and virtual sensor (VS). The two components point in the same direction in accordance with the estimated tyres slip factors.

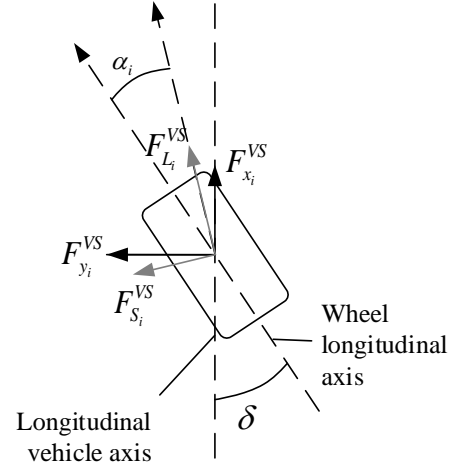


Figure 8. Illustration of the reference systems mentioned in the text. The reference rotation from the chassis ( $x - y$ ) to the wheel ( $L - S$ ) encompasses the steering angle  $\delta$  and the side slip angle  $\alpha_i$ .

## Observer calibration and validation

The observer prediction capability is assessed against a straight-line braking manoeuvre with fixed brake torque demand. For this preliminary analysis, the regenerative braking function is disabled and just the frictional brakes are used. The simulation starts with an initial vehicle speed of 20 m/s, afterwards the driver induces a base brake situation.

The Figure 9, reports a comparison between the developed wheel torque observer and IPG CarMaker simulation results for base braking manoeuvre. The displayed signals refer to the front left wheel (FL). The first graph reports the states of vehicle kinematics and the tire-road friction contact limit. The  $a_x$  and  $\mu_{lim}$  signals are conveniently scaled in order to facilitate the reading. In the central graph, the longitudinal force acting on the front left wheel is shown with reference to respectively, longitudinal virtual sensor signal (VS), Kalman filter (KF) and the IPG simulation reference force (sim). The graph at the bottom displays the observed and the simulated torque for the front left wheel. The RMSE (round mean square error) is used to evaluate the performance of the developed observer. In the discrete form, RMSE can be stated as:

$$RMSE_{T_{wheel_i}} = \sqrt{\frac{\sum_{k=1}^n (T_{wheel_{i,k}} - \hat{T}_{wheel_{i,k}})^2}{n}} \quad (15)$$

Wherein,  $k$  is an index ranging among the  $n$  simulation point and  $T_{wheel}$  and  $\hat{T}_{wheel}$  represent respectively the wheel torque simulated and the estimated. This equation can be more conveniently expressed as a percentage of the mean torque value.

With reference to the previous simulation, by applying the eq. (15), the RMSE results equal to 19Nm (6%). It is worth remarking that the virtually estimated longitudinal force is more accurate than the modelled one. Therefore, the Kalman filter is tuned in order to yield the sensors measurement.

Another simulation is performed to validate and test the compensation capability of the Kalman filter against changing road conditions. During the braking action, the vehicle crosses a slippery surface that induces a rapid deterioration of the maximum contact force. The results are reported in the Figure 10. Similarly to the previous, the upper figure reports the vehicle kinematics states and the tire-road friction contact limit. In the central graph, the longitudinal force acting on the front left wheel is represented according to the longitudinal virtual sensor signal (VS), Kalman filter (KF) with and without correction factor and the IPG simulation reference force (sim). Hereunto, the latter graphs demonstrates that the observer with road disturbance compensation ensures better results since the correction factors allows the filter to quickly adapt to changing road conditions. The correction equations, (13) and (14), make up for variation of road conditions by conveniently scaling the longitudinal tyre forces. The compensation feature attains a 50% reduction of the RMSE in regard to the wheel torque observation.

Before proceeding, it is worth remarking that the wheel torque represents the result of the sum of the electric and frictional torque whereas the estimation of the brake linings friction coefficient draws upon the frictional torque component. This latter can be easily evaluated by subtracting the regenerative torque, estimated as function of the generated current, from the observed wheel torque.



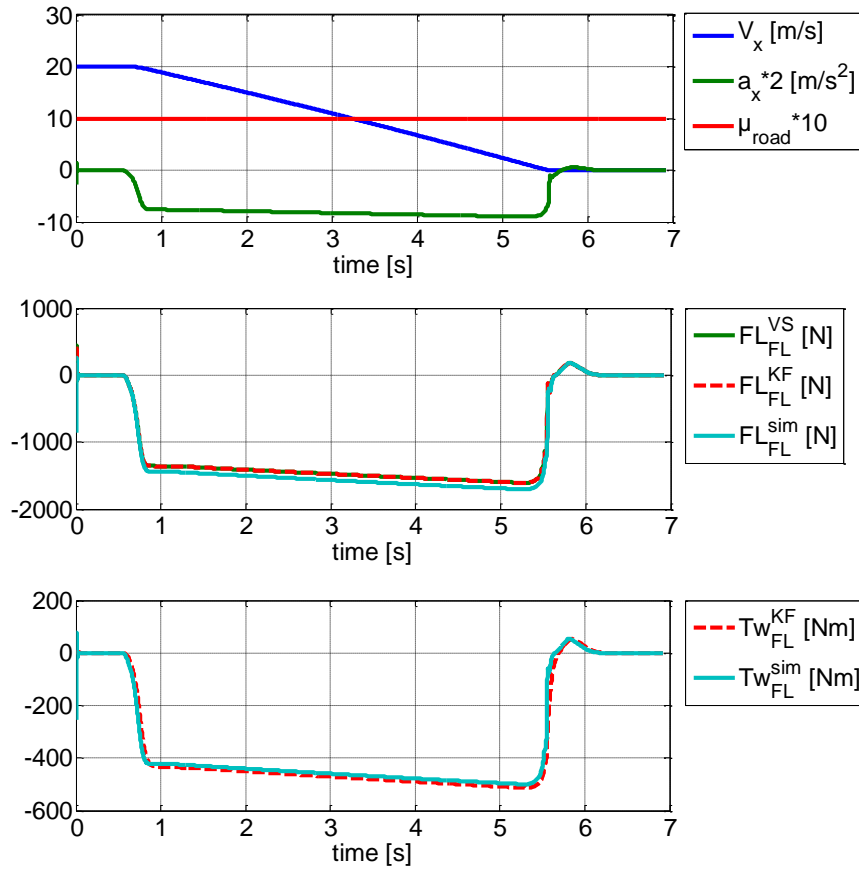


Figure 9. Comparison between developed wheel torque observer and IPG simulation results for a base braking manoeuvre. In the upper graph vehicle kinematics is shown in terms of speed and acceleration profiles; also the tire-road friction contact limit is reported. In the central graph, the longitudinal force acting on the front left wheel is shown with reference to respectively the longitudinal virtual sensor signal (VS), Kalman observer (KF) and the IPG simulation reference force (sim). The latter graph displays the comparison between the observed and the simulated torque for the front left wheel.



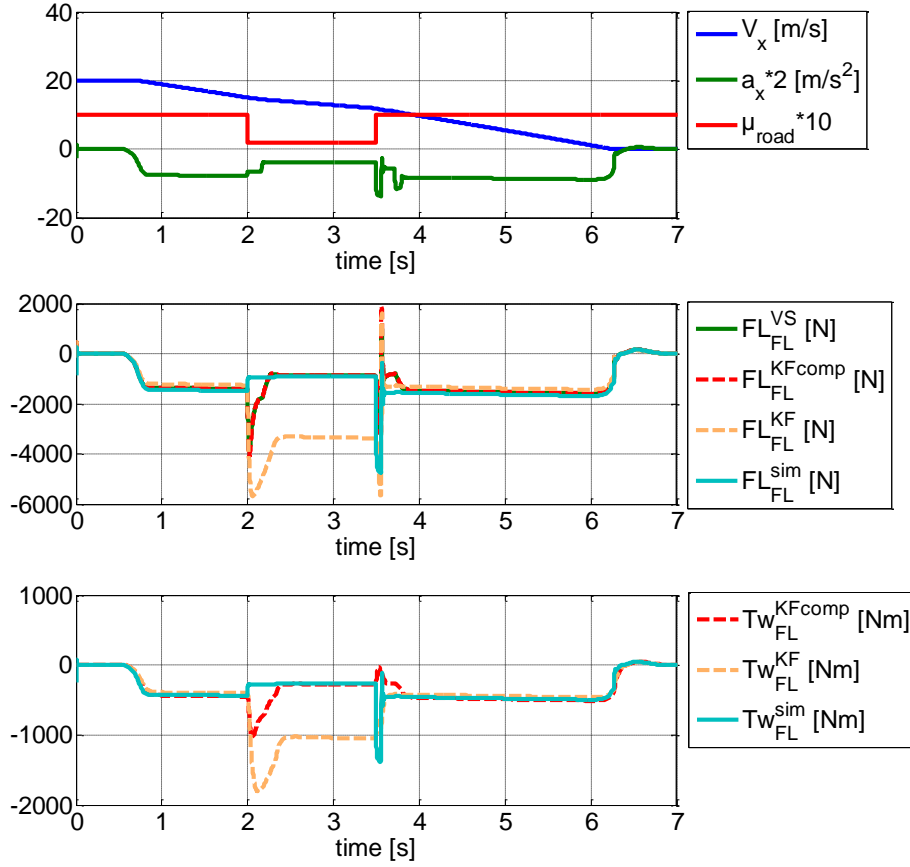


Figure 10. Comparison between developed wheel torque observer and IPG simulation results for a base braking manoeuvre with changing road conditions. During the braking manoeuvre, the vehicle crosses a slippery surface with friction limit equal to 0.2. The upper graph reports the vehicle kinematics states, namely the vehicle longitudinal speed and acceleration. In addition, the tire-road friction contact limit is reported. In the central graph, the longitudinal force acting on the front left wheel is represented according to the longitudinal virtual sensor signal (VS), Kalman observer (KF) with and without correction factor and the IPG simulation reference force (sim).

## Friction Coefficient Estimation

Once the wheel torque has been observed, the estimation of the brake friction coefficient is easily achievable: (i) the signal of the brake pressure ( $p_{brake_i}$ ) is provided by the EHB control unit; (ii) the clamping force radial application point ( $r_b$ ) is assumed known. Hence:

$$T_{brake\_FR_i} = 2 \cdot \mu_{brake_i} \cdot r_b \cdot A_{cyl} \cdot p_{brake_i} \quad (16)$$

In order to avoid the numerical problem that would arise from a direct algebraic division between the observed torque and the measured braking pressure, the Recursive Least Square method (RLS), without forgetting factors, is applied on a defined set of  $N$  time samples to evaluate the brake linings

coefficient of friction. With reference to each wheel, eq. (16) can be rewritten in a general form as:

$$\begin{Bmatrix} y_1 \\ \vdots \\ y_k \\ \vdots \\ y_N \end{Bmatrix}_i = \begin{Bmatrix} \Phi_1 \\ \vdots \\ \Phi_k \\ \vdots \\ \Phi_N \end{Bmatrix}_i \theta_i \quad (17)$$

Whereby, for the matter in hands at the generic time step  $k$ :

$$y_{k,i} = T_{brake\_FR_{k,i}} \quad (18)$$

$$\Phi_{k,i} = 2 \cdot r_b \cdot A_{cyl} \cdot p_{brake_{k,i}} \quad (19)$$

$$\theta_i = \mu_{brake_i} \quad (20)$$

The estimated value of  $\theta_i$  is calculated as:

$$\theta_i = (\bar{\Phi}_i^T \bar{\Phi}_i)^{-1} \bar{\Phi}_i^T \bar{y}_i \quad (21)$$

In the Figure 11 a comparison between the estimated and simulated brake linings coefficient of friction for several blending conditions is reported. The prediction capability is estimated as a percentage of the RMSE between the estimated and simulated brake friction coefficient. The displayed signal refers to the front left wheel. The performed simulation involves an initial vehicle speed of 72km/h and initial brake temperature of 150°C; afterwards the driver induces a brake base maneuver characterized by a constant brake pedal position of 60%. For each simulation, the demanded torque remains the same, resulting in the same vehicle deceleration profile.

It is worth noticing that higher grades of electric motor intervention produce a deterioration on the estimator prediction capability. In fact, the friction coefficient estimation through the eq. (21) is slightly deteriorated when the frictional brake torque demand is confined to low values. Regardless, the prediction capability with reference to the investigated blending conditions exhibits a RMSE lower than 8%.

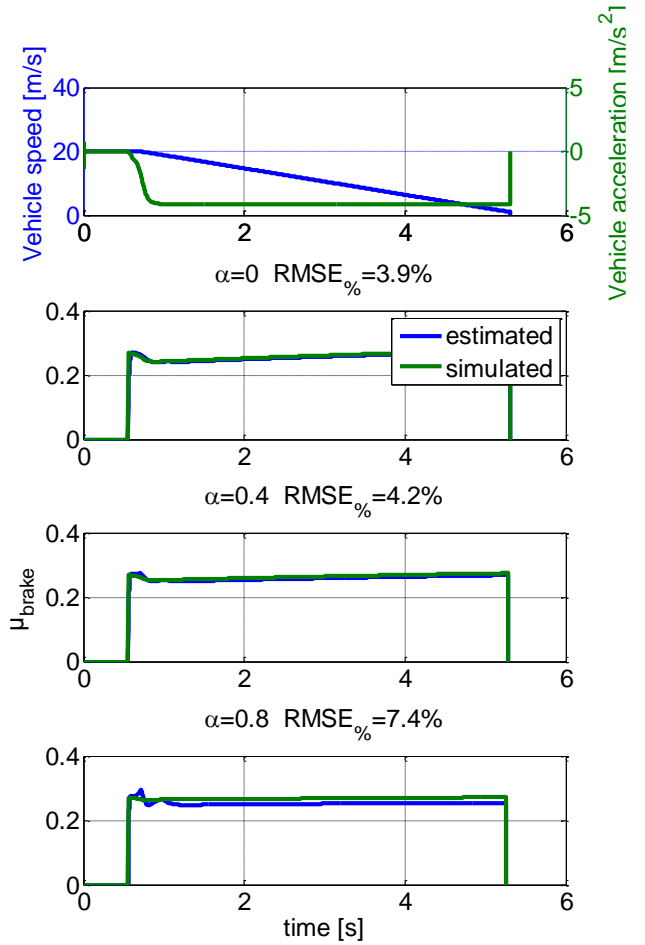


Figure 11. Comparison between simulated and estimated brake linings coefficient of friction for three different blending situation. The simulation concerns a straight line braking maneuver with a vehicle initial speed of 72km/h and initial brake temperature of 150°C.

## Compensation function

In this section, the compensation function is tested and assessed against dynamic simulations conducted through the IPG proprietary software. Particularly, two simulation tests are here analysed. The former involves a straight line braking manoeuvre with an initial velocity of 72km/h and an initial brake temperature of 150°C. A first trial with pure intervention of the frictional brake system is presented but, in the second instance, several blending conditions are investigated.

The second tests include a series of braking manoeuvres in order to induce an increase of the brake temperature and a noticeable variation of the brake linings coefficient of friction. The vehicle starts from an initial speed of 130km/h and the brakes are at an initial temperature of 150°C. Moreover, the test involving the braking series is conducted for two blending configurations, viz. full frictional brake intervention ( $\alpha = 0$ ) and blending at 70% ( $\alpha = 0.7$ ), in order to assess the system compensation capability for different working conditions. For both the simulation tests, the driver pedal displacement is limited to 60% of the maximum travel in order to induce base braking and prevent wheel lock.

The tests are performed against three braking situations, namely under-braking, over-braking and compensated case. The definition of the latter cases arises from the introduction of an ideal case of braking without any disturbances where the vehicle realises the same deceleration as demanded by the driver. Further on, the compensation mechanism will be assessed and compared with the ideal case and the conventional cases without compensation.

The results of the first test are reported in the Figure 12. The upper graph refers to the vehicle kinematics for the three braking situation, instead the lower graph puts into comparison the simulated friction coefficient with reference to the front left wheel. Moreover, also the estimated friction coefficient, provided for the compensation feature in the brake base controller, is reported. It is worth reminding that for this simulation, pure intervention of the frictional brake system is considered ( $\alpha = 0$ ).

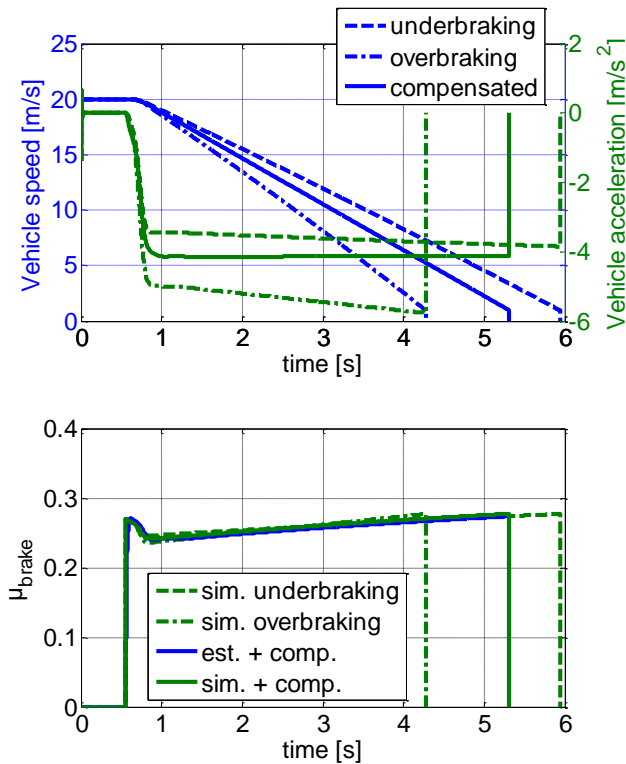


Figure 12. A straight line braking maneuver is performed in order to assess the compensation capability of the proposed approach and its repercussion on the driving feeling. No blending is enabled during this simulation. The upper graph displays the vehicle kinematics with respect to the three operating conditions. The lower graph compares the simulated friction coefficient for the front left wheel. Moreover, the estimated friction coefficient used for the compensation function is also reported.

Once, assessed the estimation capability of the developed approach, the previous test is repeated for different blending configurations. This time, the compensation capability of the proposed approach is quantified through the percentage

RMSE between the overall demanded and simulated torque. As shown in the Figure 13, the compensation abates the error between the driver requested deceleration (brake pedal actuation) and the actual deceleration level. It is clear that, since all the sources of disturbances are attributed to the variations of the brake linings coefficient of friction; the more the electric motor intervention is privileged, the less the disturbances will take a toll on the brake control.

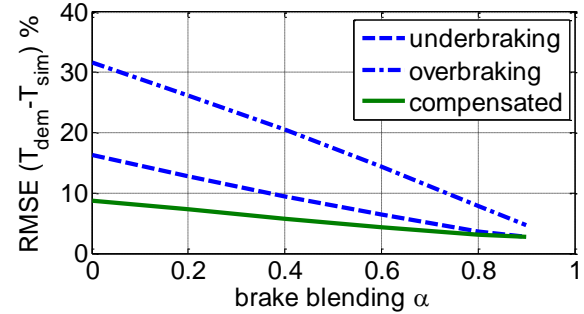


Figure 13. The compensation drastically abates the error between the demanded and the simulated overall torque, resulting in an improved driving comfort and better system response.

The second test is performed in order to assess the compensation feature even in case of manoeuvres encompassing several pedal actuations and marked variation of the brake linings coefficient of friction. The results of this trial are reported in Figure 14 and Figure 15, respectively for the case of pure conventional brake intervention and blending at 70%. The latter value has been experimentally identified at the Technische Universität Ilmenau using the HIL technique with real brake system and emulated electric propulsion system as a good compromise between the energy recuperation and brake performance [4]. With reference to the figures, representative respectively of  $\alpha = 0$  and  $\alpha = 0,7$ , it is worth remarking that the developed tool exhibit high accuracy; indeed, the estimated coefficient of friction lays close to the simulated profile in the compensated case.

Hereunto, one of the main characteristics that is worth comparing is the brake pedal travel against the vehicle acceleration during the brake manoeuvre. These curves are reported at the bottom of Figure 14 and Figure 15. For the non-compensated cases the load on the driver is increased since the respective curves are far from the ideal profile (red curve). Particularly, in the under-braking case (dash line), higher brake pedal travel must be applied to realize the same deceleration level. Conversely, in the over-braking case (dash-dot line), the same pedal actuation produces higher deceleration levels. In the non-compensated cases, the deviations in deceleration are directly dependent on the current value of the brake linings coefficient of friction. The compensation algorithm detecting a friction loss event aligns the pedal travel-deceleration curve to the ideal profile. Therefore, the curve for the compensated case (solid line) lays closer to the ideal characteristic.

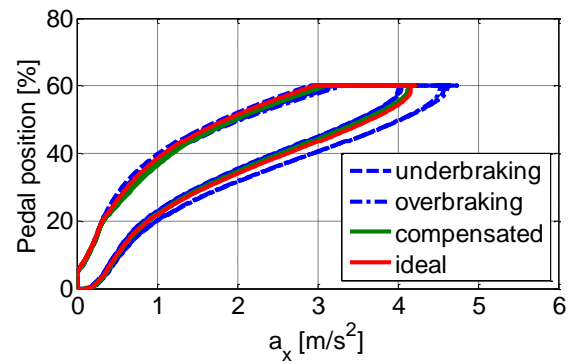
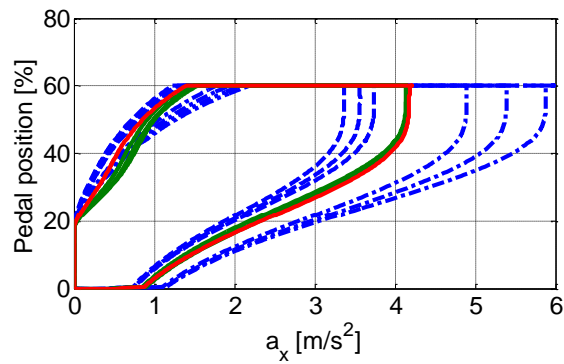
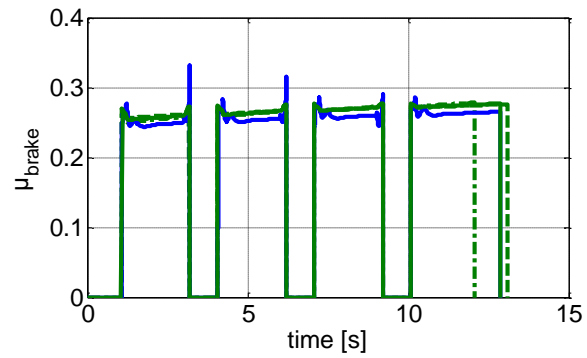
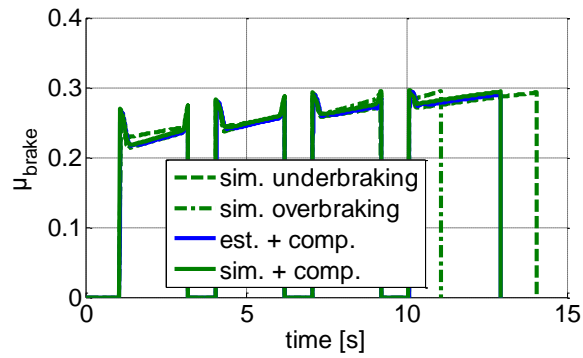
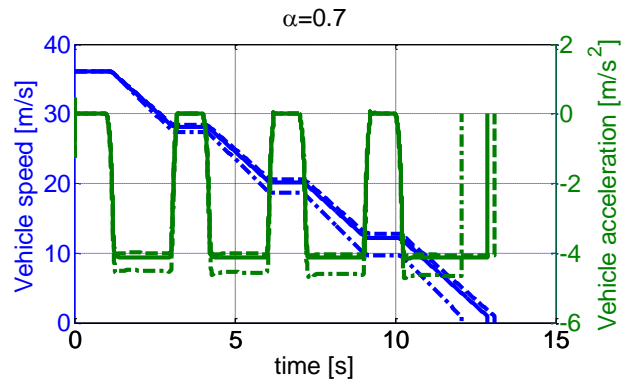
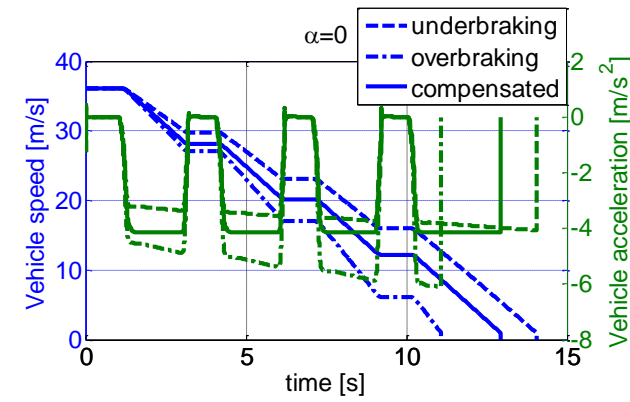


Figure 14. Comparison among the three braking situation with disabled blending function. The first graph represents the vehicle kinematics data with reference to the three operating cases. The graph in the center reports the simulated friction coefficient for both the under-braking and over-braking cases and both the estimated and simulated friction coefficient when the compensation function is enabled. The last graph represents the acceleration-pedal position characteristic curve for the different operation modes; moreover, also the ideal case is reported.

Figure 15. The same analysis is conducted by enabling the regenerative brakes with blending factor equal to 70%.

## Summary/Conclusions

The presented paper introduces a method for compensating disturbances arising from unexpected variations of the brake linings coefficient of friction. This compensation feature has been developed for the decoupled EHB system of a fully electric vehicle equipped with four in-wheel motors. A vehicle simulator from the proprietary software IPG has been used for the implementation of the brake base controller, observer of the wheels torque and estimator of brake linings coefficient of friction. Moreover, experimental results from brake dynamometric test rig are considered in the vehicle dynamics simulation software to reproduce the real behaviour of brake linings coefficient of friction.

The compensation mechanism draws upon the observation of the wheel torque through a linear Kalman filter. The observer uses measurement coming directly from the vehicle sensors; it requires low computational burden and guarantees robustness and reliability against variations of the plant characteristics due to brake wear itself or in case of replacement with aftermarket brake linings. As demonstrated, the observer here developed is capable of providing an accurate estimation of the wheel torque even in presence of disturbances induced by variations of road conditions.

Thereafter, an estimation technique based on the RLS has been developed to evaluate the actual brake friction coefficient once the wheel torque is observed, the clamping force is measured and the radial position of the clamping force application point is known. The estimated friction coefficient is provided to the brake blending control block in order to properly update the torque demand.

Straight-line braking manoeuvres have been performed in the simulation software in order to assess the compensation function. The simulation results confirm the functionality of the developed wheel torque observer and disturbance compensator. The compensation mechanism during brake torque generation in presence of brake blending allows the enhancement of brake performance and comfort by reducing the driver workload.

Further investigations will include an experimental assessment of the developed controller on the HIL facilities available at Technische Universität Ilmenau and a more detailed study of the system robustness against external disturbances.

## References

- [1] S. Amara, G. Pita-Gil, T. Raste and B. Bayer, "Electric vehicles, a new opportunity for brake by wire systems," *Proc. of 16th International SIA Conference in Vehicle Dynamics*, pp. Mulhouse, France, 2011.
- [2] G. Freitag, M. Gerlich, D. Bergmann, G. Pais and B. Fischer, "Replacement of the friction brake by a wheel hub drive," *Proc. of the 3rd International Munich Chassis Symposium chassi.tech plus*, pp. Munich, Germany, 2012.
- [3] V. Ivanov, D. Savitski, K. Augsborg and P. Barber, "Electric vehicles with individually controlled on-board motors: Revisiting the ABS design," in *IEEE International Conference on Mechatronics*, 2015.
- [4] B. Shyrokau, D. Savitski, D. Wang, V. Ivanov and K. Augsborg, "Analysis of coordination and novel blending strategy between friction brake system and electric motors," in *Eurobrake 2013 Conference*, Dresden, 2013.
- [5] N. Mutoh, "Driving and Braking Torque Distribution Methods for Front and Rear Wheel Independent Drive Type Electric Vehicles on Roads with Low Friction Coefficient," *IEEE Transactions on Industrial Electronics*, 59 (10), pp. 3919-3933, 2012.
- [6] M. Rosenberger, R. Uhlig, T. Koch and M. Lienkamp, "Combining Regenerative Braking and Antilock Braking for Enhanced Braking Performance and Efficiency," *SAE Technical Paper 2012-01-0234*, 2012.
- [7] J. Balotin, P. Neis and N. Ferreira, "Analysis of the influence of temperature on the friction coefficient of friction materials," in *ABCM Symposium Series in Mechatronics*, 4, Rio de Janeiro, 2010.
- [8] F. Talati and S. Jalalifar, "Analysis of heat conduction in a disk brake system," *Heat Mass Transfer*, 45, pp. 1047-1059, 2009.
- [9] M. Eriksson, F. Bergman and S. Jacobson, "On the nature of tribological contact in automotive brakes," *Wear*, 252, pp. 26-36, 2002.
- [10] B. Shyrokau, D. Wang, K. Augsborg and V. Ivanov, "Vehicle Dynamics with Brake Hysteresis," *Proceeding of the Institute of Mechanical Engineers, Part D: Journal of Automobiles Engineering*, 227(2), pp. 139-150, 2013.
- [11] D. Hess and A. Soom, "Friction at a lubricated line contact operating at oscillating sliding velocities," *Journal of Tribology*, 112, pp. 147-152, 1990.
- [12] D. Thuresson, "Thermomechanical analysis of friction brakes," in *Proceedings of the 18th Annual Brake Colloquium and Engineering Display*, San Diego, CA, 2000.
- [13] D. Chan and W. Stachowiak, "Review of automotive brake friction materials," *Proceedings of Institution of Mechanical Engineers, Part D: Journal on Automobile Engineering*, 218, pp. 953-963, 2004.
- [14] D. Simon, *Optimal state estimation: Kalman, H infinity, and nonlinear approaches*, John Wiley & Sons, 2006.
- [15] D. Savitski, B. Shyrokau and V. Ivanov, "Base-Brake Functions of Electric Vehicle: Disturbance Compensation in Decoupled Brake System," *International Journal of Vehicle Design*, 2015.
- [16] C. Lee, D. Savitski, C. Manzie and V. Ivanov, "Active Brake Judder Compensation Using and Electro-Hydraulic Brake System," *SAE International Journal of Commercial Vehicles*, 8(1), pp. 20-26, 2015.
- [17] H. B. Pacejka, *Tire and Vehicle Dynamics*, Third Edition, Oxford: Butterworth-Heinemann, 2012.
- [18] G. Ostermeyer, "On the dynamics of the friction coefficient," *Wear*, 254, pp. 852-858, 2003.
- [19] K. Augsborg, D. Savitski, L. Heidrich and V. Ivanov, "Combined Testing Technique: Development of Friction Brake System for Electric Vehicle," *SAE Technical Paper*, 2014.

- [20] W. Cheney and D. Kincaid, Numerical Mathematics and Computing, Thomson Brooks/Cole, 2008.
- [21] L. Ray, "Nonlinear tire force estimation and road friction identification: simulation and experiments," *Automatica*, 33(10), pp. 1819-1833, 1997.
- [22] S. Müller, M. Uchanski and K. Heidrick, "Estimation of the maximum tire-road friction coefficient," *Journal of dynamic systems, measurement, and control*, pp. 607-617, 2003.
- [23] R. Rajamani, G. Phanomchoeng, D. Piyabongkarn and J. Y. Lew, "Algorithms for real-time estimation of individual wheel tire-road friction coefficients," *IEEE/ASME Transactions on Mechatronics*, 17(6), pp. 1183-1195, 2012.
- [24] M. Doumiati, A. Victorino, A. Charara and D. Lechner, "Estimation of vehicle lateral tire-road forces: a comparison between extended and unscented kalman filtering," *IEEE Control Conference (ECC)*, pp. 4804-4809, 2009.
- [25] H. Hamann, J. K. Heidrick, S. Rhode and F. Gauterin, "Tire force estimation for a passenger vehicle with the unscented kalman filter," *IEEE Intelligent Vehicles Symposium Proceedings*, pp. 814-819, 2014.
- [26] G. H. Hostetter and J. S. Meditch, "On the generalization of observers to systems with unmeasurable, unknown inputs," *Automatica*, 9(6), pp. 721-724, 1973.
- [27] S. S. Haykin, Kalman filtering and neural networks, New York: Wiley, 2001.
- [28] U. Kiencke and L. Nielsen, Automotive control systems: for engine, driveline, and vehicle, Springer Science and Business Media, 2005.
- [29] M. Doumiati, A. Victorino, A. Charara, G. Baffet and D. Lechner, "An estimation process for vehicle wheel-ground contact normal forces," *IFAC Proceedings Volumes*, 41(2), pp. 7110-7115, 2008.

## Contact Information

Vincenzo Ricciardi, MSc, Automotive Engineering Department,  
Technische Universität Ilmenau

e-mail: [vincenzo.ricciardi@tu-ilmenau.de](mailto:vincenzo.ricciardi@tu-ilmenau.de)

## Acknowledgments

This work has been carried out within the iTEAM (Interdisciplinary Training Network on Multi-Actuated Ground Vehicles) with financial support provided by the European Community Horizon 2020 Framework Programme under grant agreement No. 675999.